NJC

Accepted Manuscript

This article can be cited before page numbers have been issued, to do this please use: T. Nyokong, M. Kimura, N. Kobayashi and G. G. Matlou, *New J. Chem.*, 2017, DOI: 10.1039/C7NJ01716B.

ROYAL SOCIETY OF CHEMISTRY

rsc.li/njc

View Article Online
DOI: 10.1039/C7NJ01716B

Journal Name

ARTICLE

Synthesis and Photophysical studies of asymmetric zinc phthalocyanine - magnetic nanoparticles conjugates.

Received 00th January 20xx,
Accepted 00th January 20xx

DOI: 10.1039/x0xx00000x

www.rsc.org/

Gauta Gold Matlou, [a] Nagao Kobayashi, [b*] Mutsumi Kimura[b] and Tebello Nyokong[a*]

This work reports on the synthesis and amide bond linkage of carboxylic acid functionalized asymmetric zinc phthalocyanine (ZnPc) complexes to amino magnetic nanoparticles (AMNPs). The work further compares the photophysical and photochemical parameters of the Pc complexes alone with the linked to form ZnPc-AMNPs with further relation to the type of the spacer between the Pc and the AMNPs. Infrared spectroscopy confirmed the presence of the amide bond formed between Pc complexes and AMNPs. Triplet quantum yields ranged from 0.62 to 0.87. However, low singlet oxygen quantum yields were obtained due to competing pathways and the insufficient energy transfer from the excited triplet state of the ZnPc molecules to the molecular oxygen.

Introduction

Metalphthalocyanines (MPcs) are versatile macrocycles that have attracted attention for various applications including in photodynamic therapy (PDT) [**1,2**], photodynamic antimicrobial chemotherapy (PACT) [**3**], photoelectrochemistry and photovoltaics [**4,5**]. Depending on the central metal, MPcs are efficient at generating singlet oxygen [**6**] which is essential for their application as photosensitizers in applications such as in PACT and PDT.

Studies on the conjugates between MPcs and nanoparticles (NPs) are on the increase. The NPs improve the photophysical parameters of the phthalocyanine complexes [**7,8**]. Iron oxide (Fe_2O_3) magnetic nanoparticles (MNPs) have attracted attention in biology and engineering due to their biocompatibility, biodegradability and ease of functionalization [**9**]. MPcs have been linked to Fe_3O_4 MNPs for photocatalytic applications or photophysical studies [**10–15**]. MNPs are also attractive because they encourage intersystem crossing (ISC) to the triplet sate of the Pc, through the external heavy atom effect of the metals contained in the MNPs. This enhances the singlet oxygen generating ability of the Pc [**13,14**], which is fundamental to applications of Pcs as photosensitizers. In addition, the use of MNPs allows for magnetic retrieval of the photocatalyst following photocatalysis [**15**].

This work reports on the synthesis of carboxylic functionalized mono zinc phthalocyanine complexes and their conjugation to amino functionalized MNPs (AMNPs). Zinc phthalocyanines (ZnPc) possess high triplet and singlet oxygen quantum yields [**16**], hence ZnPc derivatives are employed in this work. The complexes employed in this work are shown in Fig. 1. Complexes **5** and **6** are reported in this work for the first time whereas the synthesis of complex **7** has been reported before [**17**]. The photophysical properties of conjugates of porphyrin (similar in structure to Pcs) with MNPs are affected by the length of the spacer between the two [**18**], hence we compare the effect of the extra double bond between the Pc and COOH groups by comparing complexes **6** and **7.** We further compare the effect of tert-butyl groups by comparing the photophysical behaviour of **5** with **7**. Asymmetric phthalocyanines offer a more defined coordination to the nanoparticles because of their one arm of attachment, this is the reason why this study focuses on using asymmetric phthalocyanine. In addition, previous reports have shown that asymmetry improves the photophysical properties of porphyrin-type complexes [**19**]. The bulky tert-butyl substituents for **5** help in improving solubility and reducing aggregation. The COOH group for **5**, **6** and **7** will be used to link the Pcs to AMNPs.

Experimental

Materials

Zinc chloride, zinc acetate ($Zn(OAc)_2$), dimethyl sulfoxide (DMSO) and dimethyl formamide (DMF), 1,3-diphenylisobenzofuran (DPBF), 1-pentanol, p-coumaric acid

[a] *Centre for Nanotechnology Innovation, Department of Chemistry, Rhodes University, Grahamstown 6140, South Africa*

[b] *Department of Chemistry and Materials, Faculty of Textile Science and Technology, Shinshu University, Ueda 386-8567, Japan*

Corresponding Author: T. Nyokong (t.nyokong@ru.ac.za)

View Article Online
DOI: 10.1039/C7NJ01716B

(**2b**), N, N'-dicyclohexylcarbodiimide (DCC) and N-hydroxysuccinimide (NHS), and 1.2 dicyanobenzene (**4b**), were purchased from Sigma–Aldrich. Methyl 4-hydroxybenzoate (**2a**), dimethylaminoethanol (DMAE) and 4-tertbutylphthalonitrile (**4a**), were purchased from Wako chemicals**.** Tetrahydrofuran (THF) was purchased from MINEMA. 4-Nitro phthalonitrile (**1**) was synthesized according to the method published in literature [**20**]. The syntheses of amino functionalized magnetic nanoparticles (AMNPs) [**21**] and zinc mono carboxyphenoxy phthalocyanine (ZnMCPPc) (**7**) [**17**] have been reported.

Equipment

The ground state electronic absorption was measured using Shimadzu UV-2550 spectrophotometer. Fluorescence excitation and emission spectra were collected on a Varian Eclipse spectrofluorometer using a 360-1100 nm filter. The excitation spectra were measured using the Q-band of the emission maxima. Time Correlated Single Photon Counting (TCSPC) setup (FluoTime 200, Picoquant GmbH) was used for the fluorescence decay studies. The excitation source was a diode laser (LDH-P-670 driven by PDL 800-B, 670 nm, 20 MHz repetition rate, 44 ps pulse width, Picoquant GmbH).

Bruker Alpha FT-IR spectrophotometer with universal attenuated total reflectance (ATR) was used to measure the FT-IR spectra. Bruker Autoflex III smartbeam TOF/TOF Mass spectrophotometer was used to collect mass spectra data using α-cyano-4-hydrocinnamic acid as the matrix in the positive ion mode. Elemental analysis (CHNS microanalysis) was recorded using the Vario-Elementar Microcube ELIII. Bruker AMX 300 and Bruker AVANCE 600 MHz Hz nuclear magnetic resonance (NMR) spectrometers were used to measure the ^{1}H NMR spectra.
Transmission electron microscope (TEM) images were obtained using a JEOL TEM 1210 transmission electron micro-scope at 100 kV accelerating voltage. TEM samples were prepared on the sample grid and allowed to dry before measurements. X-ray powder diffraction (XRD) patterns were recorded on a Bruker D8 Discover equipped with a Lynx Eye detector, using Cu K α-radiation (λ = 1.5405 Å, nickel filter). The XRD data were fitted using Eva (evaluation curve fitting) software. Baseline corrections were performed on each diffraction pattern. Dynamic light scattering (DLS) experiments were conducted on a Malvern Zetasizer Nanoseries, Nano-ZS90.

Triplet quantum yields were determined using laser flash photolysis system. The excitation pulses were produced using a tuneable laser system consisting of an Nd: YAG laser (355 nm, 135 mJ/4-6 ns) pumping an optical parametric oscillator (OPO, 30 mJ/ 3-5 ns) with a wavelength range of 420-2300 nm (NT-342B, Ekspla). Triplet lifetimes were determined by exponential fitting of the kinetic curve using OriginPro 8 software. For laser flash photolysis studies, the samples and the ZnPc standard solutions had an absorbance of ~ 1.5 at the Q band. The solution was then introduced into a spectrophotometer cell of 1 cm path length and de-aerated using argon for 15 min. The complexes and conjugates were excited at the crossover wavelength of the Q band maxima of both the standard and the samples, and there is low scattering by the MNPs at this wavelength.
Photocatalysis for singlet oxygen quantum yield studies were carried out using irradiation from a halogen lamp (300 W), 600 nm glass (Schott) and water were used to filter off ultra-violet and far infrared radiation respectively. An interference filter (Intor, 670 nm with bandwidth of 40 nm) was placed in the light path just before the sample. Light intensities were measured with a POWER MAX 5100 (Molelectron detector Incorporated) power meter and were found to be 9.42 x 10^{18} photons/cm^2 s for singlet oxygen studies. For singlet oxygen quantum yield determinations, samples or ZnPc standard at an absorbance of ~ 1.5 at the Q band were mixed with DPBF at a ratio of 1: 1 and the rate of degradation of the DPBF photobleaching agent for both the sample and the standard were used to calculate the singlet oxygen quantum yields.

Synthesis

Phthalonitriles (3a and 3b)

Scheme 1 illustrates the synthesis of **3a** and **3b** by base catalysed nucleophilic nitro displacement of nitro group from 4-nitrophthalonitrile (**1**) with hydroxyl containing substituents (using **2a** and **2b,** respectively). Both reactions were carried out at room temperature under inert gas with constant stirring. Typically, for the synthesis of compound **3a,** (Scheme 1, route (a))**,** 3.0 g (0.017 mol) of **1** was reacted with 2.64 g (0.017 mol) of **2a** and 3.52 (0.026 mol) of dry K_2CO_3 in 20 mL of dry DMSO for 48 h to yield 3.58 g (75% yield) of compound **3a**. Compound **3b,** (Scheme 1, route (b)) was synthesized by reacting 2.01 g (0.011 mol) of **1** with 1.89 g (0.011 mol) of **2b** and 1.50 g (0.010 mol) of dry K_2CO_3 in 20 mL of dry DMSO for 48 h to yield 2.18 g (67% yield) of **3b**. **3a** was washed and precipitated out of the reaction mixture by propanol and finally recrystallized twice with hot methanol. **3b** was precipitated using ice water containing a few drops of hydrochloric acid. The precipitate was filtered, washed with water and recrystallized twice with methanol.

3a, Yield = 75%. IR (ATR): 2230 cm^{-1} (C=N), 2959, 3079 cm^{-1} (C-H), 1710 cm^{-1} (C=O), 1240 cm^{-1} (Ar-O-Ar). ^{1}H NMR (300 MHz, $CDCl_3$) δ 7.71 (d, *J* = 8.7 Hz, 2H), 7.42 – 7.11 (m, 4H), 6.88 (s, 1H), 2.11 (s, 3H). Calcd for $C_{16}H_{10}N_2O_3$: C (69.06); H (3.62); N (10.07); Found C (68.34); H (3.05); N (11.02).
3b, Yield: 67 %. FTIR (ATR), cm^{-1}. 3302 (Carboxylic OH), 3060 (Ar-H), 2232 (C=N), 1705 (C=O), 1622 (C=C), 1589 (Ar-C=C), 1253 (Ar-O- Ar). ^{1}H NMR (300 MHz, DMSO) δ 12.46 (s, 1H, -OH), 7.81 (d, *J* = 1.0 Hz, 2H), 7.48 (dd, *J* = 8.05, 3.24 Hz, 4H, Ar-H), 7.42 (d, *J* = 1.0 Hz, 2H, Ar-H), 7.21 (s, 1H, Ar-H). Calcd for $C_{17}H_{10}N_2O_3$: C (70.34), H (3.47), N (9.65); Found C (69.55), H (3.63), N (9.22).

View Article Online
DOI: 10.1039/C7NJ01716B

Synthesis of asymmetric phthalocyanines

Scheme 1 illustrates the synthesis of asymmetrically substituted Zinc phthalocyanine derivatives. Mixed condensation reaction involving two phthalonitriles (**4a** and **3a** for **5**(Scheme 1, route (a))**;** or **4b** and **3b** for **6** (Scheme 1, route (b)) was used to achieve the desired asymmetrical zinc phthalocyanine derivative. In a typical synthesis of **5a** and **5**, compound **4a** (0.460 g, 0.0025 mol) was reacted with **3a** (0.440 g, 0.0015 mmol) in a glass tube reactor containing dry dimethyl amino ethanol (DMAE) (1 mL) and dry zinc acetate (0.15 g, 0.008 mol). The reactions were carried out at 160 °C in an argon atmosphere for 7 h with constant stirring to yield 62.28 mg (11%) of **5a** after multiple column chromatography separation from mixed products using silica gel as stationary phase and 2% methanol in dichloromethane as eluting solvent. Hydrolysis of **5a** to yield mono functionalized carboxylic acid Pc (**5**) was achieved by reacting **5a** (50 mg) with 3 M KOH in 2 mL dry tetrahydrofuran and 2 mL of methanol for 24 h at 70 °C. The product (**5**) was then precipitated and filtered out of the reaction mixture by adding few drops of acetic acid and excess amounts of water to yield 26 mg (52%) of **5**. The synthesis of **6** was also carried out by using mixed condensation of two phthalonitriles as follows: **4b** (0.320 g, 2.5 mmol) and **3b** (0.435 g, 1.5 mmol) were mixed with zinc chloride (0.20 g,1.5 mmol) in 2 ml 1-pentanol. The reaction was carried at 160 °C for 7 h catalysed with few drops of DBU. The desired product (**6**) was separated from the mixture by extensive column chromatography with silica stationery phase and 5 % methanol in THF as the eluting solvent.

5a, Yield = 11%. UV/Vis (DMSO) λ_{max} / nm (Log ε): 676(5.02), 610(4.41), 351(4.73). IR (ATR): 2963 cm^{-1} (C-H), 1711 cm^{-1} (C=O), 1493 cm^{-1} (Ar-C=C), 1242 cm^{-1} (C-N). ^{1}H NMR (600 MHz, DMSO) δ 8.31 (d, *J* = 2.0 Hz, 6H, Pc-Ar), 8.02 (s, 1H, Pc-Ar), 7.71 (s, 3H, Pc-Ar), 7.62 (d, *J*=2.8 Hz, 2H, subs-Ar), 7.32 (d, *J* = 1.8 Hz, 2H, subs-Ar), 7.29 (d, *J* = 2.3 Hz, 2H, Pc-Ar), 3.75 (s, 3H, -OCH_3), 1.35 (s, 27H, -CH_3). MALDI-TOF MS (m/z): Calcd 944.49; Found 940 [M - 4H]$^-$. Calcd for $C_{52}H_{46}N_8O_3Zn$: C (69.68); H (5.17); N (12.50); Found C (69.31); H (5.05); N (13.30).

5, Yield = 52%. UV/Vis (DMSO) λ_{max} / nm (Log ε): 677 (4.71), 611 (4.32),352 (3.99).IR (ATR): 3310 cm^{-1} (OH), 2961 cm^{-1} (C-H), 1708 cm^{-1} (C=O), 1497 cm^{-1} (Ar-C=C), 1236 cm^{-1} (C-N).^{1}H NMR (600 MHz, DMSO) δ 9.10 (s, 1H, -OH), 8.29 – 8.16 (m, 8H, Pc-Ar), 7.97 (s, 3H, Pc-Ar), 7.81 (s. 1H, Pc-Ar), 7.53 (dd, *J* = 8.3, 2.2 Hz, 4H, subs-Ar), 1.34 (s, 27H, -CH_3). MALDI-TOF MS (m/z): Calcd 930.46: Found 931 [M + 1H] $^+$. Calcd for $C_{51}H_{44}N_8O_3Zn$: C (69.42); H (5.03); N (12.70); Found C (68.83); H (5.46); N (11.22).

6, Yield = 17 %, UV/Vis (DMSO) λ_{max} / nm (Log ε): 675 (5.54), 608 (4.77), 352 (5.01). IR (ATR): 3290 (Carboxylic O-H), 3090 (Ar-H), 1712 (Carboxylic C=O), 1475 (Ar-C=C), 1661 (C=C), 1233 (C-N). ^{1}H NMR (600 MHz, DMSO) δ 12.45 (s, 1H, OH), 8.13 (d, *J* = 8.8 Hz, 2H, Pc-Ar), 7.91 – 7.77 (m, 8H, Pc-Ar), 7.62 (d, *J* = 16.0 Hz, 2H, Pc-Ar), 7.50 – 7.43 (m, 3H, Pc-Ar), 7.22 (dd, *J* = 8.7,4.3 Hz, 4H, Subs-Ar), 6.57 (s, 1H, -C=C), 6.51 (s, 1H, -C=C). MALDI-TOF MS (m/z): Calcd: 740, Found: 742 [M + 2H] $^+$. Calcd for $C_{41}H_{22}N_8O_3Zn$: C (66.54), H (3.00), N (15.14): Found C (65.48), H (3.13), N (14.56).

Conjugation of Pc complexes to magnetic nanoparticles

Typically, **5** (20 mg, 0.023 mmol), **6** (20 mg, 0.027 mmol) and **7** (20 mg, 0.028 mmol) were reacted with DCC (4.74 mg, 0.023 mmol for **5**, 8.66 mg, 0.042 mmol for **6**, 16.09 mg, 0.078 mmol for **7**) and NHS (2.55 mg, 0.023 mmol for **5**, 4.84 mg, 0.042 mmol for **6**, 3.22 mg, 0.028 mmol for **7**) in dry DMF (2 mL) for 48 h to activate the carboxylic group on the Pc complex. After 48 h, AMNPs (20 mg for all complexes) in dry DMF (2 mL) were added and the mixture was left stirring for a further 72 h to allow formation of the amide bond between NH_2 groups of the magnetic nanoparticles and the phthalocyanine carboxylic group. The conjugates were purified from the reaction mixture by centrifuging with DMF, twice with water, twice with methanol and twice with ethanol.

Photophysical studies and Photochemical Parameters

The fluorescence (Φ_F), singlet oxygen (Φ_Δ) and triplet (Φ_T) quantum yields of **5**, **6**, **7**, **5**-AMNPs, **6**-AMNPs and **7**-AMNPs were determined using comparative methods reported in literature [**22–25**]. Unsubstituted ZnPc dissolved in DMSO was used as reference standard (Φ_F =0.2 [**23**] , Φ_T^{Std} = 0.65 [**24**] and Φ_Δ^{Std} = 0.67 in DMSO [**25**]).

View Article Online
DOI: 10.1039/C7NJ01716B

Results and Discussions

Synthesis and characterization

The synthesis of the phthalonitrile complexes **3a** and **3b** is illustrated on Scheme 1. The infrared spectra of compound **3a** and **3b** indicated the presence of the nitrile (C=N) peaks at 2230 and 2232 cm^{-1}, respectively. The carbonyl peaks (C=O) were observed at 1710 cm^{-1} for **3a** and 1705 cm^{-1} for **3b**. Ar-O-Ar stretch at 1240 cm^{-1} (**3a**) and 1253 cm^{-1} (**3b**) results from the ether bond between the two benzene rings and confirms the structures of **3a** and **3b**. The ^{1}H NMR spectra for compounds **3a** and **3b** gave signals between 6.88 ppm to 7.81 ppm resulting from the two aromatic rings. Complex **3a** had a multiplet (7.42 – 7.11 ppm) which integrated into 4 protons from the phenoxy ring, a doublet at 7.71 ppm and a singlet at 6.88 ppm which integrated into two protons and a single proton, respectively, which completes the phthalonitrile phenyl ring. The methyl protons gave a singlet peak at 2.11 which integrated into 3 protons. **3b** had a broad singlet peak at 12.46 ppm representative of the carboxylic hydroxyl peak which integrated into a singlet proton. The cinnamic acid phenyl ring gave a doublet of a doublet at 7.48 ppm which integrated into 4 protons, while the unsaturated carbons gave a doublet peak at 7.42 ppm, which integrated to give 2 protons completing the protons on the cinnamic acid substituent. The phthalonitrile phenyl ring gave doublet peak at 7.81 ppm that integrated into 2 protons and a singlet at 7.21 ppm which integrated into a single proton which completes the protons of the second ring for **3b**. The elemental analysis of both the phthalonitrile gave the values in agreement with analytically calculated values.

A_3B type ZnPc were synthesized in this work. Tertiary butyl phthalonitrile (**4a**) and 1.2 dicyanobenzene (**4b**) were used as the A_3 while (**3a**) and (**3b**) were used as the B diiminoisoindoline of the Pc complex. Scheme 1 illustrates the synthesis of **5a** and **5** and **6** phthalocyanine derivatives. The FTIR spectra of the complexes **5a** and **5** indicate the unsaturated (C-H) carbon stretching bands at 2963 cm^{-1} (for **5a**) and 2961 cm^{-1} (for **5**) from the tert-butyl substituents. The appearance of the broad hydroxyl stretching band at 3310 cm^{-1} for **5**, indicated the successful hydrolysis of **5a** to **5**. Also, Peaks at 3290 cm^{-1} for **6**, together with the 3310 cm^{-1} for **5** are indicative of the presence of the carboxylic hydroxyl groups, see Fig. 2. The carbonyl stretching bands were observed between 1708-1712 cm^{-1} for all complexes (**5a**, **5** and **6**). The Pc core IR peaks were indicated by the aromatic carbon-carbon (Ar-C=C) stretching bands at 1493 cm^{-1} (**5a**), 1497 cm^{-1} (**5**) and 1475 cm^{-1} (**6**) together with the carbon-nitrogen (C-N) peaks at 1242 cm^{-1} (**5a**), 1236 cm^{-1} (**5**) and 1233 cm^{-1} (**6**). The successful synthesis of the Pc complexes was also confirmed by an absence of C=N peaks between 2232 and 2240 cm^{-1} which were present in the phthalonitriles (precursors).

^{1}H NMR of the **5a** and **5** complexes varied only by the appearance of the broad singlet peak at 9.10 ppm for **5** which is absent in **5a**, thus confirms the presence of hydroxyl groups and the successful hydrolysis of **5a** to **5**. The Pc-core aromatic protons of **5a** were between 7.29 ppm and 8.31 ppm all integrating to 12 protons while the other protons resulted from the aromatic ring of the substituents: 7.32 ppm, (2 protons) and 7.62 ppm (2 protons), the methoxy group (3.75 ppm, 3 protons) and the tertiary butyl groups (1.35 ppm, 27 protons), all accounting to 46 protons contained on **5a** complex. **5,** gave a broad singlet peak at 9.10 ppm which confirms the presence of the carboxylic acid after hydrolysis of **5a**. The aromatic signal**s** of the complex were indicated by the presence of a multiplet peak at 8.29 - 8.16 ppm, a singlet at 7.81 ppm and another singlet at 7.97 ppm which completes all 12 protons of the Pc core aromatic rings. The aromatic ring of the substituent groups gave a doublet of doublets (at 7.53 ppm) which integrated to four protons that completes the aromatic ring of the substituent. The tertiary butyl groups gave a sharp singlet peak at 1.34 ppm which integrated to 27 protons, thus completing the 44 protons of the **5** complex. The H NMR spectrum for complex **6** is provided in **supporting information Fig. S1** and showed expected peaks. The elemental analysis of the complexes (**5a**, **5** and **6**) gave percentages that are in close to the analytically calculated percentages.

View Article Online
DOI: 10.1039/C7NJ01716B
Journal Name ARTICLE

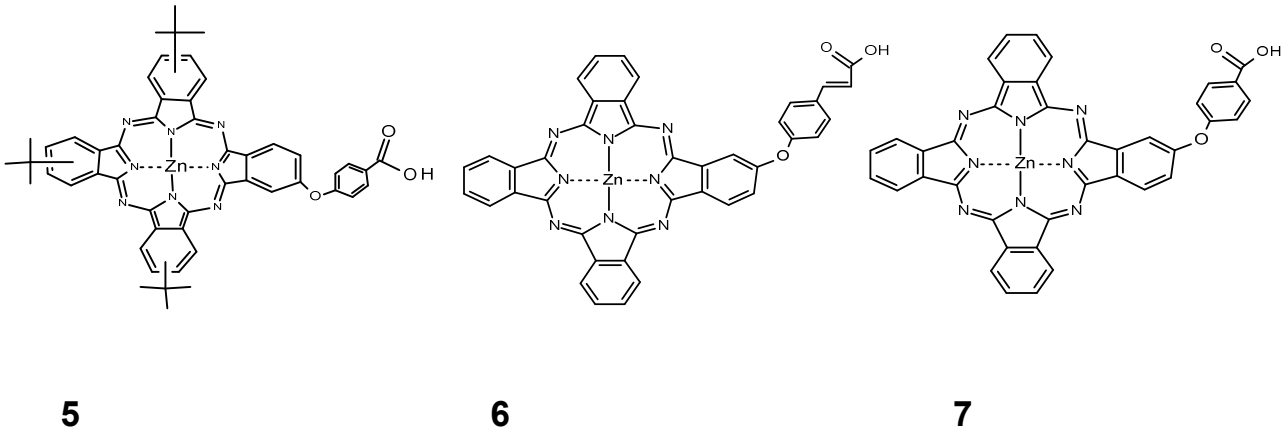

Figure 1. Structure comparison of the phthalocyanines to be used in this work

Conjugation of Pc complexes to AMNPs.

Scheme 2 illustrates the method used to covalently link the Mono-Pc complexes (**5**, **6** and **7**) onto the surface of the AMNPs through an amide bond using DCC and NHS as the coupling and stabilizing agents respectively. Asymmetric Pc complexes are only able to link through one attachment side. The number of Pc molecules bonded to the AMNPs was determined following literature methods, but using absorption instead of fluorescence [**26**]. This involves comparing the Q band absorbance intensity of the Pc in the conjugate with that of the initial Pc before the conjugation. The ratio of AMNPs: Pc is then determined and listed in Table 1. Approximately the same number of Pcs are linked to each MNP.

The FTIR spectra of the complexes **5, 6**, **7**, **5**-AMNPs, **6**-AMNPs and **7**-AMNPs are illustrated in Fig. 2. The peaks of interest which suggest the successful linkage of the AMNPs to the asymmetric carboxylic containing phthalocyanine complexes can be seen at 1540 and 1640 cm^{-1} which represent an amide (N-H) spike and an amide carbonyl carbon respectively. It must be noted that the carboxylic hydroxyl groups (at ~ 3000 cm^{-1}) of **5**, **6** and **7** disappear after conjugation to AMNPs because of the formation of the covalent bond and loss of water during the coupling reaction to give **5**-AMNPs, **6**-AMNPs and **7**-AMNPs. The observation of an amide bond in the infrared spectra provided evidence for the successful linkage of the Pc complexes to the AMNPs.

View Article Online
DOI: 10.1039/C7NJ01716B

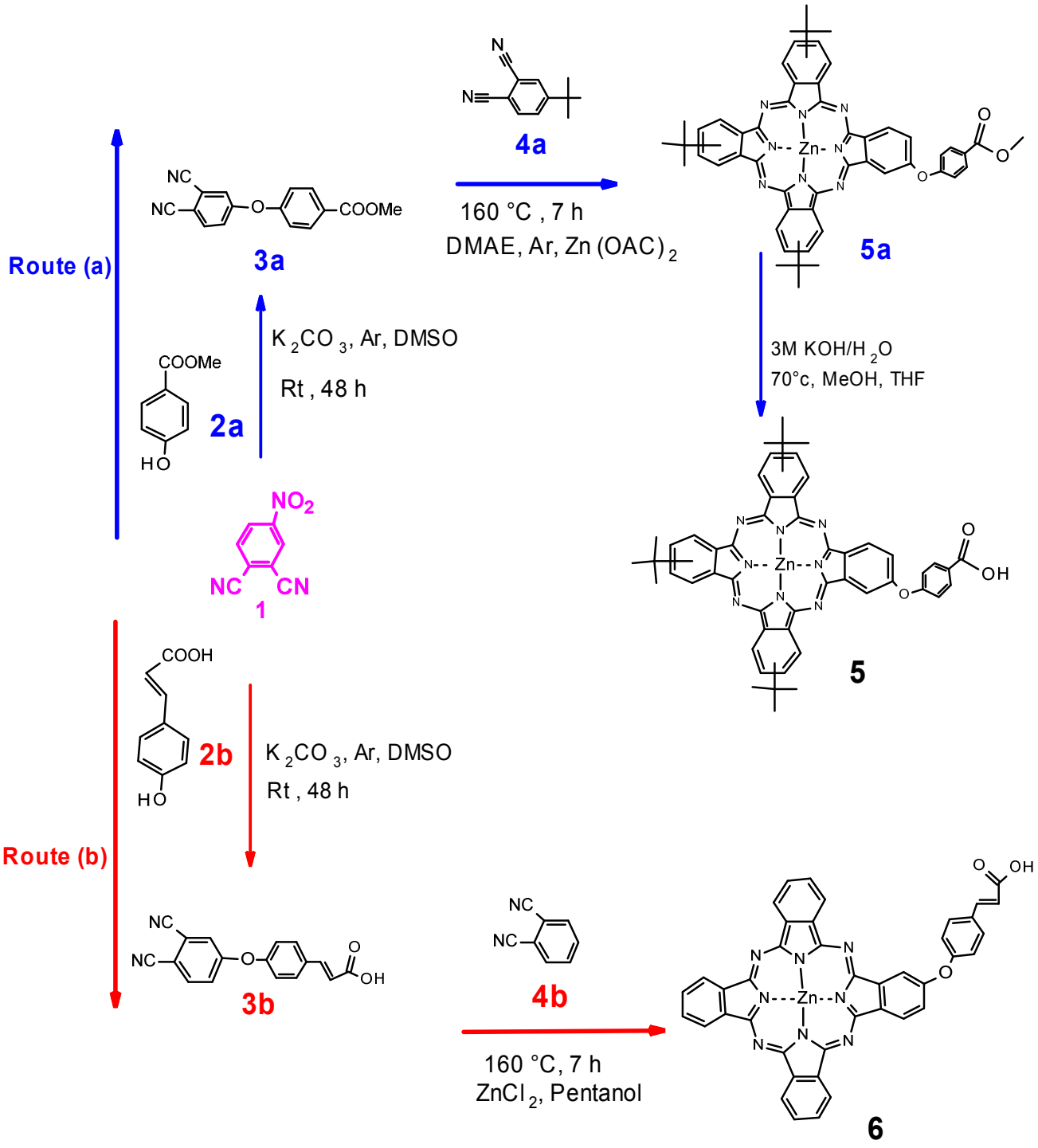

Scheme 1 : Schematic illustration of the synthesis of complexes **5** (Route (a) and **6** (route (b) and their precursors.

View Article Online
DOI: 10.1039/C7NJ01716B

Journal Name

ARTICLE

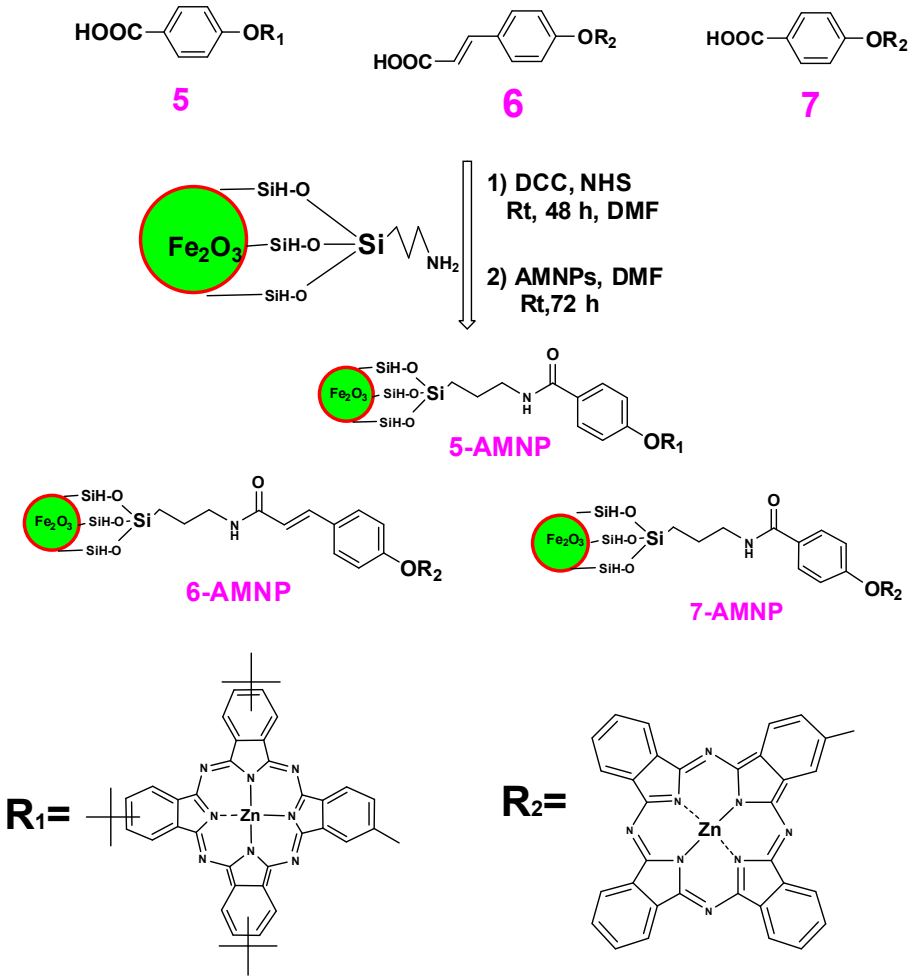

Scheme 2: Schematic illustration of the conjugation of AMNPs to carboxylic

View Article Online
DOI: 10.1039/C7NJ01716B

Journal Name

ARTICLE

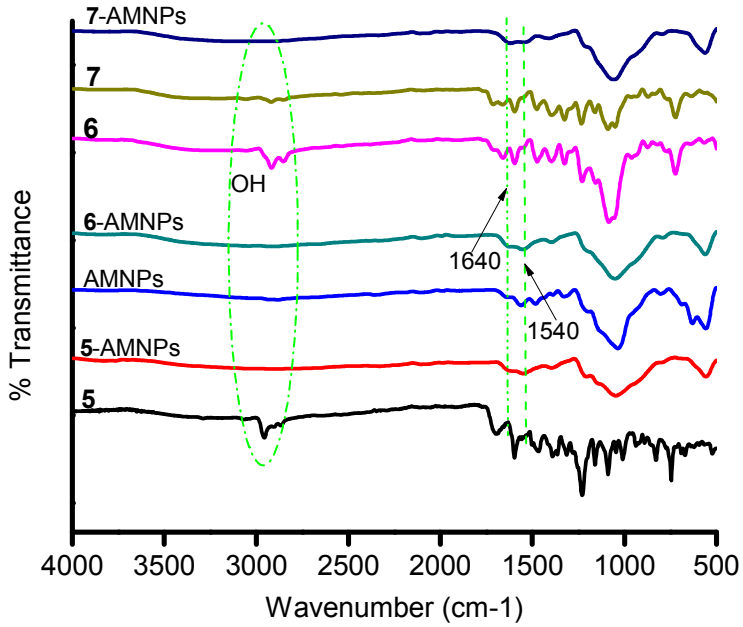

Figure 2: Infrared spectra of complexes **5**, **6** and **7** with their respective conjugates **5**-AMNPs, **6**-AMNPs and **7**-AMNPs.

TEM images of the nanoparticles are illustrated on Fig.S2 (supporting information). The images reflect spherically shaped nanoparticles. The magnetic nature of the particles makes them to be attracted to each other forming clusters, **Fig. S2**. The AMNPs, Fig. S2A, had an average size of 13.89 nm, Table 1. The TEM images of the conjugates (Fig S2 B-D,) showed an increase in size together with the presence of sheet like structures which can be attributed to the Pc complexes linked on the surface of the nanoparticles. Interactions between the Pcs on adjacent NPs via π-π stacking may occur leading to aggregation. Pcs are known for their π-π stacking to form H aggregates [**27**].

The XRD spectroscopy was used to show the changes in the crystal structure of the AMNPs upon linkage to the Pc complexes. The XRD patterns of the complexes (**5** as an example of the ZnPc derivatives) and the conjugates (**5**-AMNPs, **6**-AMNPs, **7**-AMNPS) are illustrated in Fig. 3. The AMNPs have a face centred cubic structure with diffraction peaks at 2θ = 30°, 36°,43°, 54°,57° and 63°, corresponding to hkl Milner indices of 220, 311, 400, 422, 511 and 440, respectively. The broad peak near 2θ = 15° for Pc alone is typical of phthalocyanines due to their amorphous nature [**28**]. After conjugation, the MNPs diffraction peaks were clearly observable on the pattern of **5**-AMNPs, **6**-AMNPs and **7**-AMNPs. The XRD patterns of the conjugates (**5**-AMNPs, **6**-AMNPs and **7**-AMNPs) also shows the Pc diffraction peak at 2θ = 15°. The sizes of the AMNPs and their conjugates were determined using a Debye-Scherrer equation 1 [**29**].

$$d = \frac{k\lambda}{\beta Cos\theta} \qquad 1$$

where d is the crystal size, λ is the wavelength of the X-ray source (λ =1.5405˚A, nickel filter), k is an empirical constant equal to 0.9, β is the full width at half maximum of the diffraction peak and θ is the diffraction angle of the crystal orientation peak. The sizes of the AMNPs and their conjugates are listed in Table 1. Upon conjugating to Pc-complexes, the crystal size of the AMNPs increases because of the Pc incorporated on the surface of the nanoparticle, due to aggregation as stated above.

View Article Online
DOI: 10.1039/C7NJ01716B

Journal Name

ARTICLE

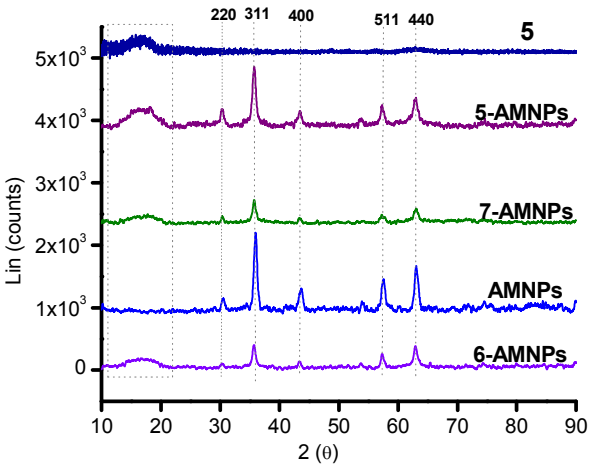

Figure 3: X-ray diffraction patterns of **5**, **5**-AMNPs, **7**-AMNPs, AMNPs, and **6**-AMNPs.

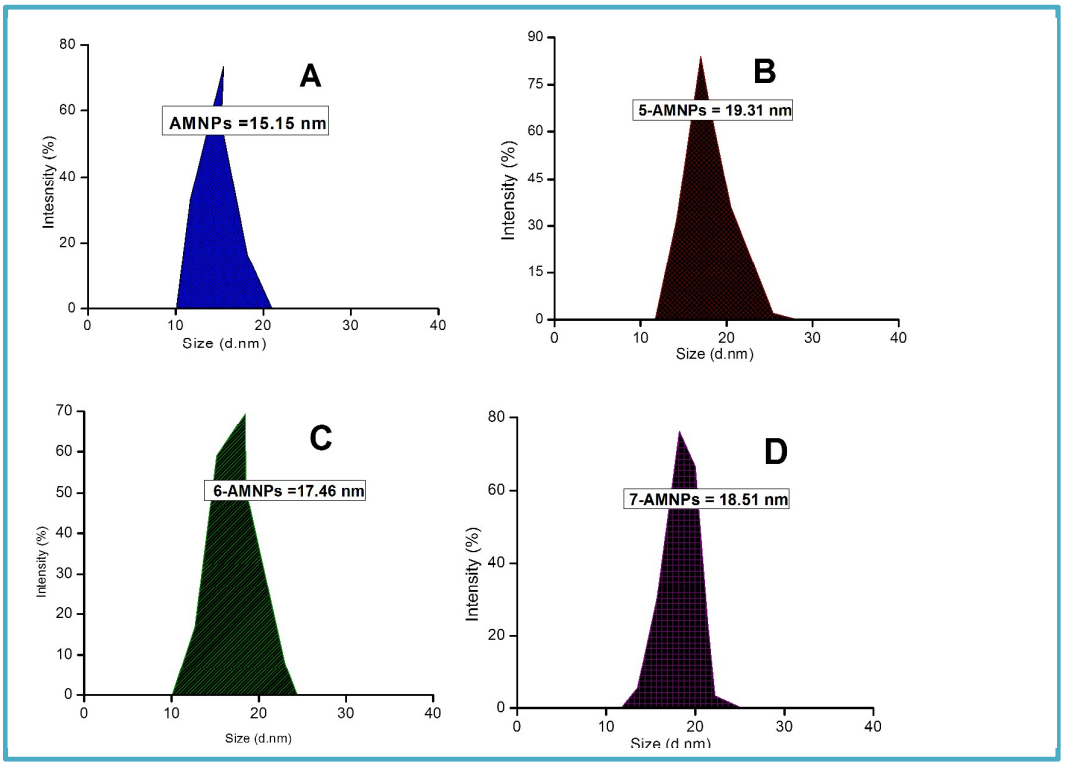

Figure 4: DLS graphs showing the average size distributions of A) AMNPs, B) **5**-AMNPs, C) **6**-AMNPs and D) **7**-AMNPs.

View Article Online
DOI: 10.1039/C7NJ01716B

Journal Name

ARTICLE

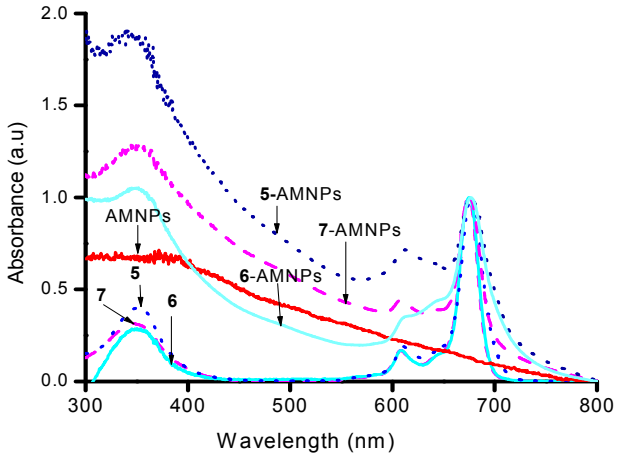

Figure 5: Electronic absorption spectra of the complexes 5, 6, 7, AMNPs, 5-AMNPs, 6-AMNPs and 7-AMNPs in DMSO.

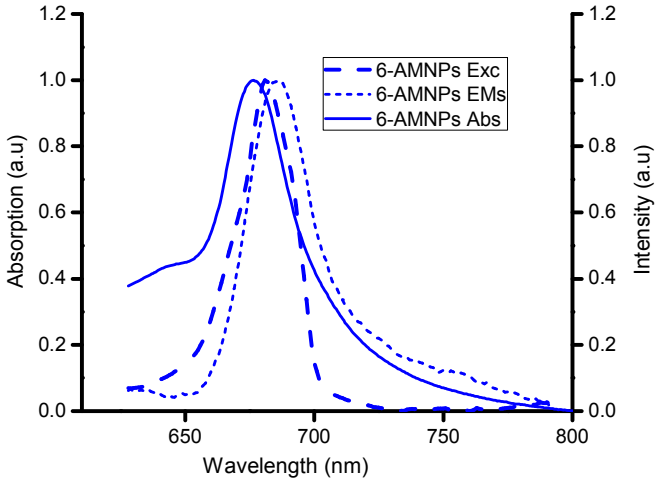

Figure 6: Absorption, emission and excitation spectra of the 6-AMNPs in DMSO. Abs = Absorption; Exc = excitation; Ems = emission

Dynamic Light Scattering (DLS) is a very sensitive technique that provides the sizes of the particles in suspension and it was used in this work to determine the size of the AMNPs alone as well for Pc-AMNPs conjugates in water. The size distributions of the nanoparticles obtained from DLS are illustrated in Fig. 4 and listed in Table 1. These results show an increase in size from 15.15 nm for AMNPS to 19.31 nm (**5**-AMNPs), 17.46 nm (**6**-AMNPs), 18.51 nm (**7**-AMNPs)) of the nanoparticles after linking the Pc complexes on the nanoparticle surface.

The electronic absorption spectra of the complexes are shown in Fig. 5. Absorption spectra which are typical of metallated phthalocyanines are observed in DMSO, with single Q-bands with maxima ranging from 674 to 677 nm (Table 1), thus there is not much difference in the Q band maxima of the three Pcs. The AMNPs showed a abroad absorption Fig. 5. The broadening below 550 nm for the conjugates is due to the presence of AMNPs showing scattering. Upon conjugation of the Pc complexes to the AMNPs, there were no significant changes in Q band maxima for **6**-AMNPs and **7**-AMNPs, Table 1.

There was a blue shift for **5**-AMNPs compared to **5** alone. The slight blue shift upon conjugation compared to Pc alone could be attributed to the electron deficiency induced on the Pcs upon coordination with NPs as reported before [**30**]. The emission and excitation spectra of the conjugates are shown in Fig. 6. The emission and excitation spectra of the conjugates were found to be mirror images of each other, Fig. 6. Slight differences in maxima between the absorption and excitation spectra could be due to different equipment used.

Photophysical and Photochemical parameters.

Fluorescence quantum yields (Φ_F) and lifetimes (τ_F)

Fluorescence quantum yields and lifetimes of the complexes are summarized in Table 1. A typical decay curve is illustrated on **Fig. S3 (supporting information)** for complex **5** (as an example). The Φ_F values are slightly lower compared to that of the ZnPc that has Φ_F = 0.2 [**23**]. The Φ_F value for **6** decreased significantly from 0.18 to 0.086 upon linking to AMNPs. A slight decrease was observed for **5**-AMNPs compared to **5**. The linkage of AMNPs to **7** did not have much influence on the Φ_F of the conjugates compared to **7** alone. The presence of the

View Article Online
DOI: 10.1039/C7NJ01716B

heavy central metal (through the heavy atom effect) accompanied by the paramagnetic nature of AMNPs is expected to encourage intersystem crossing to the excited triplet state, hence decreasing the Φ_F values of the Pc complexes [**31**] when linked to AMNPs as is case for **6** and **6**-AMNPs.

Table 1: The photophysical and photochemical parameters of ZnPc complexes together with their conjugates in DMSO.

Complex	Size (nm) TEM	Size (d) XRD (nm)	Size (nm) DLS	Loading Ratio AMNPs: Pc	λ_{Abs} (nm)	Φ_F ± 0.02	τ_F (ns)	Φ_T ± 0.05	Φ_Δ ± 0.02	τ_T (μs)
5	-	-	-	-	677	0.15	3.03	0.86	0.59	235
6	-	-	-	-	675	0.18	3.06	0.73	0.48	258
7	-	-	-	-	674	0.16	3.14	0.62	0.56	199
AMNPs	13.89	15.35	15.15	-	-	-	-	-	-	-
5-AMNPs	16.20	17.45	19.31	1: 6	673	0.11	3.62	0.87	0.47	279
6-AMNPs	16.28	18.15	17.46	1: 5	676	0.086	4.66	0.65	0.38	224
7-AMNPs	15.85	17.56	18.51	1: 5	675	0.14	3.02	0.69	0.51	256

The fluorescence lifetimes were determined from the time correlated single photon counting (TCSPc) setup. All complexes gave a single lifetime. Table 1 shows that fluorescence lifetimes lengthen for **5** and **6**, upon conjugation to AMNPs, but shorten for **7**. It is expected that fluorescence quantum yields and lifetimes should change in unison, the observed lengthening of lifetimes for complex **5** and **6** in the presence of the AMNPs may be due to the protection of the former by the latter. Complex **7** seems to behave differently with a decrease in τ_F. Magnetic cores normally quench the fluorescence of fluorophores and covalent bonding of a fluorophore such as porphyrin to MNPS *via* an appropriate spacer was reported to reduce the quenching [**32**]. Hence the differences in the behaviour of phthalocyanine in the presence of AMNPs could be related to the different interaction depending on orientation and the length of the spacer.

Triplet quantum yields and lifetimes

A comparative method using ZnPc as a standard was employed to determine the Φ_T of Pc complexes (**5**, **6** and **7**) alone and when linked to AMNPs (**5**-AMNPs, **6**-AMNPs and **7**-AMNPs), Table 1. The Pc complexes alone gave high Φ_T values with **5** = 0. 86 yielding the highest and **7** yielding the lowest at 0.62. Upon linking the Pc complexes to AMNPs, a decrease in Φ_T values for **6**-AMNPs compared to **6** is observed, while **7**-AMNPs had a slight increase in Φ_T value. There was no significant change for **5**-AMNPs. It is expected that when Φ_F decreases as is the case with **5**-AMNPs and **6**-AMNPs compared to **5** and **6**, Φ_T would increase. But this is not the case in Table 1. It is also expected that the heavy atom effect and paramagnetic nature of AMNPs would significantly increase Φ_T due to the heavy atom effect [**31**]. This is observed for **7**-AMNPs compared to **7**, Table 1, but there is a decrease of Φ_T for **6**-AMNPs compared to **6** and no change for **5**-AMNPs compared to **5**. The length of the spacer between the MNPs and porphyrins has been reported to affect photophysical parameters [**18,21**]. This could also be the case for **6**-AMNPs which has a different spacer between the Pc ring and the AMNPs compared to **7**-AMNPs and **5**-AMNPs. A longer spacer may reduce the interaction between the AMNPs and the Pc, resulting in the lowering of the heavy atom effect. However, this is not expected to quench the triplet quantum yields. MPc aggregates form through π-π stacking may quench the excited triplet state [**27**].

View Article Online
DOI: 10.1039/C7NJ01716B

Journal Name

ARTICLE

Thus, we show in this study that the heavy atom effect as well as the paramagnetic nature of the MNPs, do not always result in increased triplet state quantum yields, and that factors such as spacing between the Pc and MNPs, and aggregation take precedence.

The triplet yield lifetimes (τ_T) determine the residence time of the excited molecules in the excited state. Photosensitizers with a longer τ_T are excellent because longer τ_T allows sufficient time for energy transfer from the triplet state of the Pc to the molecular oxygen for the generation of the singlet oxygen species [**33,34**]. It is expected that when Φ_T decreases triplet lifetimes increase [**31**]. The decrease of both Φ_T and τ_T values for **6**-AMNPs could be due to aggregation as discussed above. The lengthening in τ_T in some cases could be due to the protection of the Pc by AMNP.

Singlet oxygen quantum yields (Φ_Δ)

The ability of the Pc complexes and the Pc-AMNPs conjugates to generate singlet oxygen species was evaluated using a chemical method with ZnPc as a standard and DPBF as a singlet oxygen quencher. The rate of photodegradation of DPBF was monitored by UV-Vis spectra, Fig. S4 (supporting information) using **6**-AMNPs as an example. In all cases in Table 1, there is a decrease in singlet oxygen quantum yield of the Pcs upon conjugation to AMNPs.

Triplet and singlet oxygen quantum yields are related since the latter are a result of the former interacting with ground state oxygen. The decrease in the singlet oxygen quantum yield for Pc-AMNPs conjugates could be due to the screening effect caused by AMNPs which could have prevented the interaction of the excited triplet state of the nanoconjugates and the ground state molecular oxygen [**35**] resulting in the insufficient energy transfer from the excited triplet state to the molecular oxygen. In addition, competing pathways such as nonradiative relaxation of molecules from the excited triplet state to the ground state are possible when molecules in the excited triplet state have a longer τ_T thus minimizing the efficiency of energy transfer to the molecular oxygen as indicated by the low Φ_Δ of the conjugated ZnPc complexes. It is also known that the presence of alkene double bonds results in the scavenging of singlet oxygen [**36**], hence the low value (Φ_Δ) of **6** alone or in the presence of AMNPs (**6**-AMNPs) could be due to the presence of the extra double bond. Even though there is a decrease in Φ_Δ following conjugation of ZnPc derivatives to MNPs, the presence of MNPs will allow for magnetic separation following use for applications of the conjugates for PACT or for photocatalysis, allowing for re-usability of the catalyst. In addition, MNPs have potential for use in various fields such as magnetic resonance imaging (MRI), hyperthermia and drug delivery [**37**]. Linking of phthalocyanines to MNPs allows for combination therapy using hyperthermina and PDT and for possible MRI during PDT. The Φ_Δ values of the MNPs in Table 1 are still high enough for PDT applications since PDT photosensitizers in clinical trials such as LUTRIN have Φ_Δ values as low as 0.11 [**38**].

Conclusions

Asymmetric ZnPc complexes were successfully synthesized and linked to AMNPs through an amide bond. The fluorescence quantum yields decreased significantly for 6-AMNPs compared to **6** and minimally for **5**-AMNPs and **7**-AMNPs compared to **5** and **7** respectively. The triplet quantum yields slightly increased for **7**-AMNPs compared to **7** and did not change for **5**-AMNPs compared to 5. There was a decrease in triplet quantum yield for **6**-AMNPs compared to **6** alone (containing mono coumaric acid substituent), due to aggregation and possibly due the length of the spacer between the Pc and MNPs. Nonradiative relaxation in the excited triplet state may have contributed to the limited energy transfers of ZnPc molecules to the molecular oxygen as evidenced by low singlet oxygen quantum yields especially in the presence of AMNPs. The low oxygen quantum yields of Pc-AMNPS could also be due to the screening effect.

University. We thank NRF/Japan Society for the Promotion of Science joint research program for funding.

Acknowledgements

This work was supported by the African Laser Centre (ALC), the Department of Science and Technology (DST), CSIR National Laser Centre, Rental Pool Program, National Research Foundation (NRF) of South Africa through DST/NRF South African Research Chairs Initiative for Professor of Medicinal Chemistry and Nanotechnology (UID 62620), and Rhodes

Notes and references

1 S.B Brown,E.A Brown and I. Walker, *Lancet Oncol*, 2004, **5**, 497–508.
2 L.A Muehlmann, M.C Rodrigues,J.P.F Longo, M.P Garcia, K.R Py-Daniel, A.B Veloso, P.E.N de Souza, S.W da Silva and R.B Arevedo, *J. Nanobiotechnology*, 2015, **13**, 36–47.
3 M. Wainwright, *J. Antimicrob Chemother*, 1998, **42**, 13-28.

View Article Online
DOI: 10.1039/C7NJ01716B

4 A. Kira, T. Umeyama, Y. Matano, K. Yoshida, S. Isoda, M. Isosomppi, N.V. Tkachenka, H. Lemmatyinen and H. Imahori, *Langmuir*, 2006, **22**, 5497–5503.
5 M. Idowu, T. Loewenstein, A. Hastall, T. Nyokong and D. Schlettweid, *J. Porphyr. Phthalocyanines*, 2010, **14**, 142–149.
6 K. Ishii, Coord. Chem. Rev, 2012, **256**, 1556–1568.
7 D. Bechet, P. Couleaud, C. Frochot, M.L Viriot, F. Guillemin F and M. Barberi-Heyob, *Trends Biotechnol*, 2008, **26,** 612–21.
8 T. Nyokong and E. Antunes, *Coord. Chem. Rev*, 2013, **257**, 2401–2418.
9 M. Mahmoudi, S. Sant, B. Wang, S. Laurent and T. Sen, *Adv. Drug Deliv. Rev*, 2011, **63**, 24–46.
10 C. Tshangana and T. Nyokong, *J. Fluoresc*, 2015, **25**, 199–210.
11 A.R Simioni, M.M Rodrigues, F.L Primo, P. Morais and A.C. Tedesco, *J. Nanosci. Nanotechnol*, 2011, **11**, 3604–3608.
12 D.M Oliveira, P.P MacAroff, K.F Ribeiro, Z.G.M. Lacava, R.B. Azevedo, E.C.D. Lima, P.C Morais and A.C. Tedesco, *J. Magn. Magn. Mater*, 2005, **289**, 476–479.
13 P. Modisha and T. Nyokong, *J. Mol. Catal. A. Chem*, 2014, **381**, 132–137.
14 P. Modisha, T. Nyokong and E. Antunes, *J. Mol. Catal. A. Chem*, 2013, **380**, 131–138.
15 M. Ledwaba, N. Masilela, T. Nyokong and E. Antunes, *J. Mol. Catal. A*, 2015, **403**, 64–76.
16 T. Nyokong and E. Antunes, In *The handbook of Pophrin science*, ed K.M Kadish, K.M Smith KM, Academic Press, New york, 2010, vol. 7, pp. 247-349.
17 R.O Ogbodu and T. Nyokong, *Polyhedron*, 2015, **90**, 175–182.
18 H. Gu, K. Xu, Z. Yang, C.K Chang and B. Xu, *Chem. Commun*, 2005, 4270–4272.
19 C.C Byeon, M.M McKerns, W. Sun, T.M Nordlund, C.M Lawson and G.M Gray, *Appl. Phys. Lett*, 2004, **84**, 5174–5176.
20 A. Yahyazadeh and V. Azimi, *Chem. Solid Mater*, 2012, **49**, 33–40.
21 O.L Osifeko, I Uddin, P.N Mashazi and T. Nyokong, *New J. Chem*, 2016, **40**, 2710–2721.
22 S. Fery-forgues and D. Lavabre, *J. Chem. Educ*, 1999, **76**, 1260–1264.
23 A. Ogunsipe, J. Chen and T. Nyokong, *New J. Chem,* 2004, **28**, 822–827.
24 T. Tran-Thi, C. Desforge and C. Thiec, *J. Phys. Chem,* 1989, **93**, 1226–1233.
25 N. Kuznetsova, N. Gretsova, E. Kalmykova, E. Makarova, S. Deshkevich, V. Negrimovskii V, O.L Kaliya and E.A Lukyanets, *Russ J. Gen. Chem*, 2010, **70**, 133–140.
26 L. Li , J-F Zhao, N. Won, H. Jin, S. Kim and J-Y Chen, *Nanoscale Res. Lett*, 2012, **7**, 386–393.
27 M.J Stillman and T. Nyokong, In *Phthalocyanine-properties and applications*, e.d C.C Leznoff and B. Lever, VCH, New York 1989, pp. 133–290.
28 A.W Snow, J.R Griffith and N.P Marullo, *Macromolecules* ,1984, **17**, 1614–1624.
29 R. Jenkins and R. Synder, Introduction to X-ray Diffractometry, Wiley and Sons, New York, (1996) (1998).
30 K.G Thomas and P.V Kamat, *Acc. Chem. Res,* 2003,**36**,888–98.
31 J.R Darwent, P. Douglas, A. Harriman, G. Porter and M.C Richoux, *Coord. Chem. Rev*, 1982, **44**, 83–126.
32 S.A Corr, A. O'Byrne, Y.K Gun'ko, S. Ghosh, D.F Brougham, S. Mitchell, Y. Volkov and A. Prina-Mello, *Chem. Commun,* 2006, 4474–4476.
33 A. Dudkowiak, E. Teślak and J. Habdas, *J. Mol. Struct,* 2006, **792–793**, 93–98.
34 N. Nombona and T. Nyokong, *Inorganica Chim. Acta*, 2012, **392**, 380–387.
35 E.I Sagun, E.I Zenkevich, V.N Knyukshto, A.M Shulga, D.A Starukhin and C. Von Borczyskowski, *Chem. Phys.* 2002, **275**, 211–230.
36 M.A Filatov, S. Baluschev and K. Landfester, Chem. Soc. Rev. 2016, **45**, 4668–4689.
37 S. A. Corr, Y. P. Rakovich and Y. K. Gun'ko, Nanoscale Res. Lett., 2008, **3**, 87–104.
38 R. Bonnett, In Chemical aspects of photodynamic therapy, Gordon and Breach Science Publishers, Amsterdam, 2000.